Precise Engineering of Nanocrystal Shells via Colloidal Atomic Layer Deposition

Emanuele A. Slejko,[†,‡,§] Vladimir Sayevich,[†,§] Bin Cai,[†] Nikolai Gaponik,[†] Vanni Lughi,[‡] Vladimir Lesnyak,[*,†] and Alexander Eychmüller[†]

[†]Physical Chemistry and Center for Advancing Electronics Dresden (cfAED), TU Dresden, Bergstr. 66b, 01062 Dresden, Germany
[‡]Department of Engineering and Architecture, University of Trieste, Via Valerio 6A, 34127 Trieste, Italy

Supporting Information

ABSTRACT: We present a general strategy for a facile synthesis of complex multifunctional nanoscale materials via colloidal atomic layer deposition (c-ALD). The c-ALD technique is based on self-limiting half-reactions of ionic precursors on the surface of a nanocrystal (NC) occurring at room temperature. Using this technique, uniform layers of CdS and ZnS semiconductor shells were epitaxially grown on CdSe semiconductor cores with different shell combinations, leading to the precise control of the optical properties of these heterostructures. All core–shell multicomponent nanoparticles preserve narrow size distributions, phase crystallinity, and shape homogeneity of the initial NCs. Furthermore, we attempted to extend the toolbox of the c-ALD to combine materials with intrinsically different properties, such as Au/CdS core/shell structures with substantial lattice mismatch. The results presented in this work demonstrate great opportunities for creating functional materials with programmable properties for electronics and optoelectronics.

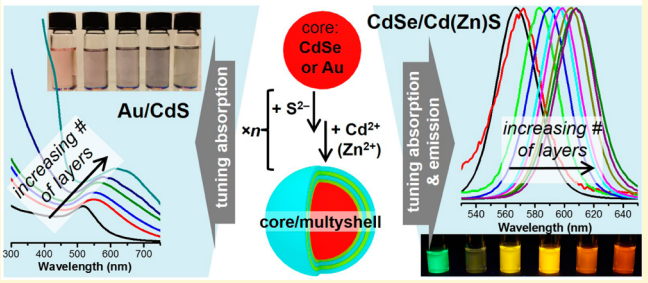

INTRODUCTION

Synthesis of colloidal inorganic nanocrystals (NCs) has experienced significant progress in past years leading to development of the synthetic methodologies for diverse nanoscale materials with unique optical and electronic properties.[1−3] One of the brightest sides of colloidally synthesized NCs is an opportunity to prepare nanomaterials with fine-tuned size, shape, composition, and complex functionalities. For example, the combination of different semiconductors in one nanoheterostructure allows us to control the confinement and topology of electron and hole wave functions, which, in turn, determine the NC properties.[4−7] Particularly, the predominant strategy for achieving higher photoluminescence (PL) is to epitaxially grow a shell of a larger band gap material around the semiconductor core (e.g., CdSe/CdS, CdSe/ZnS, CdSe/CdS/ZnS, InP/ZnS, etc.).[8,9] In these core–shell structures, the charge carrier wave functions are isolated from the surface dangling bonds, which are regarded as the main source of nonradiative pathways of exciton recombination.

Several methods for the shell formation have been developed to date, such as the heterogeneous nucleation and growth of the shell material on the surface of the core via continuous addition of precursor solutions by a syringe pump,[10−13] thermal cycling,[14,15] the successive ion layer adsorption and reaction method (SILAR),[16] and colloidal atomic layer deposition (c-ALD).[17] The latter, developed by Ithurria and Talapin, presents a new stepwise technique for the synthesis of heterostructures based on a sequential deposition of fully saturated ionic half-monolayers onto nanocrystal core seeds. This method has a number of advantages over other techniques. First, it enables easy tuning of the optical properties of the NCs while preserving their narrow size distribution and shape uniformity regardless of the initial core size, shape, concentration, and surface complexity. Second, the method offers an excellent control over the surface composition and ligand chemistry of the resulting core/shell NCs. Third, the shell grows at room temperature and shows impressive reproducibility which could be used to realize a large-scale synthesis. We note that under the c-ALD conditions it is not necessary to precisely control the concentration of initial NCs and shell precursors, since their excess is removed after each deposition step and they do not form separated nuclei at room temperature. All these make c-ALD a powerful tool to synthesize the functional units with controllable properties. Nevertheless, despite these convincing benefits, validity and versatile opportunities of the c-ALD in engineering the multifunctional materials have not been thoroughly investigated yet and so far are limited to a number of simple two-component nanoscale structures. Particularly, c-ALD was successfully implemented to grow a CdS shell on quasi-spherical CdSe[17,18] and PbS[19] NCs as well as on delicate plate-shaped CdSe NCs in solution.[17,20] Moreover, the Kagan

group used this technique in solid-phase to change the surface stoichiometry and therefore the electronic properties of PbSe and PbS NCs.[21]

In the current work we significantly extend the applicability of the c-ALD technique with the introduction of a ZnS layer that can be easily combined with a CdS layer within a complex shell on a CdSe NC core of different sizes such as CdSe/CdS3/ZnS, CdSe/CdS4, CdSe/CdS/ZnS/CdS/ZnS, CdSe/ZnS/CdS3, CdSe/ZnS4, CdSe/CdS2/ZnS/CdS, and CdSe/CdS2/ZnS2 (here the number designates the corresponding shell thickness expressed in monolayer (ML) units). This shell design results in a well-controllable modulation of the optical properties of the nanoscale materials. These NCs represent multicomponent structures with similar features, i.e., built from various semiconductors. On the other hand, the combination of materials with different nature in one heterostructure provides a higher level of compositional complexity with new properties. For instance, it was shown that synergistic properties were realized between excitons and plasmons in Au/PbS NCs.[22] However, in contrast to semiconductor−semiconductor, metal−semiconductor heterostructures usually have a large lattice mismatch between the core and shell materials. This leads to a shift of the heterogeneous nucleation energy closer to the homogeneous nucleation energy making the classical seed-mediated growth of the shell material on such cores extremely challenging.[23] As a result, the integration of dissimilar hybrid materials into one unit usually gives rise to anisotropic structures with segregation of the core and the shell materials.[24] To tackle this serious issue of the growth of uniform semiconductor outer layers on the surface of gold seeds, we also employed c-ALD. The results presented in our work undoubtedly demonstrate versatility and flexibility of the c-ALD technique to synthesize diverse heterostructures with desirable characteristics.

EXPERIMENTAL SECTION

Materials. All chemicals have been used as received, without any modification or further purification. Cadmium oxide (CdO, 99.5%), oleic acid (90%), 1-octadecene (ODE, 90%), selenium powder (99.999%), sulfur powder (99.98%), cadmium acetate dihydrate ($Cd(OAc)_2 \cdot 2H_2O$, 99.99%), zinc acetate dihydrate ($Zn(OAc)_2 \cdot 2H_2O$, 99%), *n*-methylformamide (MFA, 99%), sodium sulfide (Na_2S, 97%), tetrachloroauric acid trihydrate ($H[AuCl_4] \cdot 3H_2O$, 99.9%), *tert*-butylamine-borane complex (97%), tetraline (95−98%), oleylamine (OlAm, C18 content 80−90%), and tri-*n*-octylphosphine oxide (TOPO, technical grade) were purchased from Sigma-Aldrich. Tri-*n*-octylphosphine (TOP, 97%) was purchased from ABCR. Octadecylphosphonic acid (ODPA, 97%) was purchased from PlasmaChem.

Synthesis of CdSe and Au Nanocrystal Seeds with Quasi-spherical Morphologies. 3.3 nm CdSe NC cores have been synthesized by a hot injection process in organic media according to the published recipe.[25,26] Briefly, 90 mg of CdO, 0.5 mL of oleic acid, and 8.5 mL of ODE were mixed in a 25 mL three neck flask at 150 °C for 1 h, and then the temperature was increased to 250 °C, at which point 1 mL of the TOP-Se 1.6 M stock solution was injected. The TOP-Se stock solution was prepared by mixing 0.632 g of Se powder with 5 mL of TOP under vigorous stirring at room temperature until the solution became completely transparent. After 1 min of growth, the reaction mixture was quickly cooled to room temperature. As-synthesized CdSe NCs were precipitated with 1 mL of methanol and 3 mL of acetone, centrifuged, and then dispersed in toluene. These washing steps were repeated twice. These CdSe NC cores were used to grow CdS and ZnS shells resulting in CdSe/CdS4, CdSe/CdS/ZnS/CdS/ZnS, and CdSe/CdS2/ZnS2 colloidal heterostructures (Figure 1).

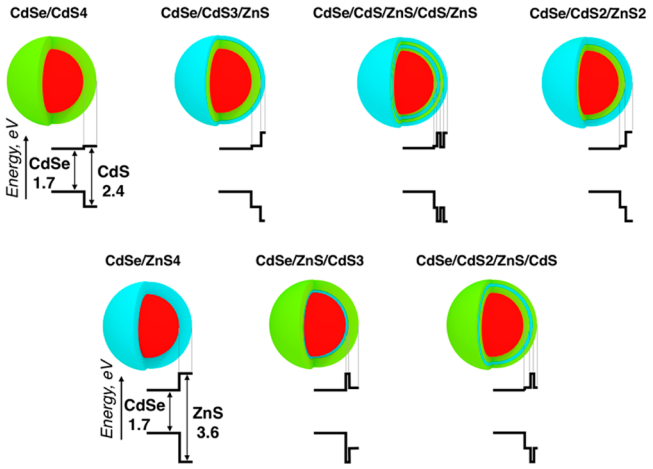

Figure 1. Scheme of the investigated shell combinations with corresponding energy band diagrams of CdSe, CdS, and ZnS. Numbers of layers are indicated after the composition with a final shell thickness of 4 MLs for all of the samples. Positions of the energy levels are depicted based on the corresponding bulk energy levels.

To demonstrate the general applicability of the c-ALD technique, we also synthesized CdSe NCs with quasi-spherical morphologies stabilized by phosphonic acids rather than by carboxylic acids, using the synthetic approach developed by Carbone et al.[27] Particularly, to obtain 3.8 nm wurtzite-type CdSe NCs, 60 mg of CdO were dissolved in 3 g of TOPO in the presence of 280 mg of ODPA at 300 °C. In this clear solution, a preprepared solution of selenium powder (58 mg) in TOP (360 mg) was injected at 330 °C and the nucleated crystals grew for 10 min. After abrupt cooling to room temperature, CdSe NCs were washed in a similar way as described above for 3.3 nm CdSe NCs. These CdSe NC cores were used to form complex multicomponent nanostructures such as CdSe/ZnS4, CdSe/ZnS/CdS3, CdSe/CdS3/ZnS, and CdSe/CdS2/ZnS/CdS.

Au spheres with diameters of ∼4 nm were synthesized according to the published recipe by Peng et al.:[28] 0.1 g of $H[AuCl_4] \cdot 3H_2O$ was dissolved in 10 mL of tetraline and 10 mL of OlAm to form a clear orange solution under argon flow. At the same time, 0.087 g of *tert*-butylamine-borane complex in 1 mL of tertaline and 1 mL of OlAm was prepared in the glovebox and swiftly injected under vigorous stirring in the Au-precursor solution at room temperature. The reaction was kept at this temperature for 1 h, and the organic-capped Au NCs were precipitated with acetone and then redispersed in hexane. The same washing steps were repeated twice using the hexane−acetone pair. The Au NCs dispersed in hexane were used as cores for the CdS shell growth.

Colloidal Atomic Layer Deposition. The c-ALD procedure followed the protocol proposed by Ithurria and Talapin.[17] Cd, Zn, and S precursors (all 0.5 M concentrations) were prepared by dissolving $Cd(OAc)_2$, $Zn(OAc)_2$, and Na_2S in MFA. Then, 0.5 mL of a 6 μM solution of quantum dots in hexane were mixed with 0.1 mL of the S-precursor and 0.5 mL fresh MFA inside a 1.5 mL plastic tube. The concentration of the CdSe NCs can be determined using molar extinction coefficients at the band-edge for a given first absorption peak energy of the NCs, as well as half-width-half-maximum of the first absorption peak and peak intensity.[29]After a few seconds phase transfer occurred and the NCs became stable in the polar solvent. These S^{2-}-terminated particles showed no PL under UV excitation. Then, washing of the obtained solution was performed, consisting of the addition of 100−300 μL of acetone to destabilize the NCs and precipitate them. Once centrifuged for 1 min at 3000 rpm, the supernatant was removed, a fresh portion of MFA was added, and the particles were redispersed by sonication. These washing steps, repeated twice after each half monolayer growth, were found to be optimal to preserve the colloidal stability of the inorganic-capped NCs while enabling the excess of unbound ionic species to be fully

removed. The latter can react with subsequently added counterions resulting in undesirable homogeneous nucleation of CdS or ZnS. Afterward, 0.5 mL of the cation precursor solution (either $Cd(OAc)_2$ or $Zn(OAc)_2$ in MFA) were added, and the mixture was vigorously shaken for 1 min to let the surface reaction occur. Once the precursor reacted with the particles, the NCs were washed again and centrifuged, and the particles were dispersed in MFA. After these two steps, one full monolayer of CdS or ZnS was grown on top of the quantum dot cores. The procedure can be repeated to reach the desired shell thickness and shell alternation.

A similar technique was implemented to grow a CdS shell around Au cores. Additionally, to improve the colloidal stability of the inorganic-capped metal−semiconductor core/shell NCs, the surface functionalization with OlAm was implemented.[30] The all-inorganic Au/CdS NCs were first precipitated from MFA solution using acetone as a nonsolvent. Then, 40 μL of OlAm in 200 μL of toluene was added to the precipitate resulting in the formation of a transparent solution of the hybrid-capped NCs. To remove the excess of OlAm, acetone was added into the NC dispersion. The dried NC powder was further redispersed in pure toluene.

Characterization. All optical spectroscopic measurements were performed at room temperature. UV−vis absorption spectra of NC dispersions were acquired using a Cary 50 spectrophotometer (Varian Inc.). A Fluoromax-4 spectrofluorometer (Horiba Jobin Yvon Inc.) equipped with a PMT detector for the visible range was used to acquire the steady-state PL spectra of the NC solutions as well as to estimate their PL quantum yields (PL QYs). To determine the PL QY of the NC dispersions, we normalized PL spectra of different samples with respect to the absorbed light intensity at the excitation wavelength and subsequently integrated the PL intensity vs photon energy over the entire spectra. The absolute values of PL QYs can be estimated by comparing the relative values with those of freshly prepared standard solutions with known QYs such as Rhodamine-101 in ethanol (99%). Rhodamine 6G in ethanol was chosen as a second standard with PL QY (96%) calculated based on Rhodamine-101 following published instructions.[31] All PL QY values were corrected for different refractive indexes of various solvents. The CdSe NC size and concentration were calculated based on the data of Jasieniak et al.[29]

Transmission electron microscopy (TEM) of the NC samples was performed using a FEI Tecnai G2 20 microscope operated at 200 kV. Specimens were prepared by dropping diluted NC dispersions on carbon-coated copper grids with subsequent evaporation of the solvent under vacuum overnight.

Powder X-ray diffraction (XRD) patterns were collected with a Bruker AXS D2 PHASER diffraction system in the reflection mode. A Nickel filter, Cu Kα1 irradiation, and a LYNXEYE/SSD160 detector were used.

RESULTS AND DISCUSSION

Multicomponent Semiconductor-Semiconductor Core/Shell Nanostructures. CdSe NCs with sizes of 3.3 and 3.8 nm were used as starting cores to synthesize core−shell heterostructured materials with a variable alternation of CdS and ZnS layers having a total shell thicknesses of 4 MLs (Figure 1). Particularly, CdSe/CdS4, CdSe/CdS/ZnS/CdS/ZnS and CdSe/CdS2/ZnS2 structures were synthesized from 3.3 nm sized CdSe NCs, while larger 3.8 nm CdSe cores were used to deposit shell layers with the formulations of CdSe/CdS3/ZnS, CdSe/ZnS/CdS3, CdSe/ZnS4 and CdSe/CdS2/ZnS/CdS. As follows from the band energy diagrams presented in Figure 1, by combining in one shell CdS and ZnS layers one can play with the band gap alignment within the resulting core/multishell heterostructures. Thus, by covering the CdSe core with either CdS or ZnS shells, the type I heterostrucure will be formed, where the band gap of the core is locked within the band gap of the shell semiconductor, confining the charge carriers inside the core. Furthermore, we can control the extent of quantum confinement by choosing a proper pair of semiconductors, i.e., compounds with the desired band alignment. For example, in the case of the CdSe/CdS structure, a hole is expected to be localized mainly in the core, whereas the electron wave function can be extended to the shell (partly delocalized) owing to a small energetic threshold between conduction bands of CdSe and CdS. Unlike in this configuration, in the CdSe/ZnS heterostructure both charge carriers should be mainly confined in the core due to relatively large energy barriers imposed by the ZnS shell depending on its thickness. Moreover, introduction of the CdS layers in between ZnS ones can yield a quantum well structure in which the larger band gap semiconductor forms energy barriers around the smaller band gap semiconductor leading to additional confinement effects.

Absorption and PL spectra of the core and core−shell NCs are presented in Figures 2 and SI1−SI6. As seen in Figure 2a,

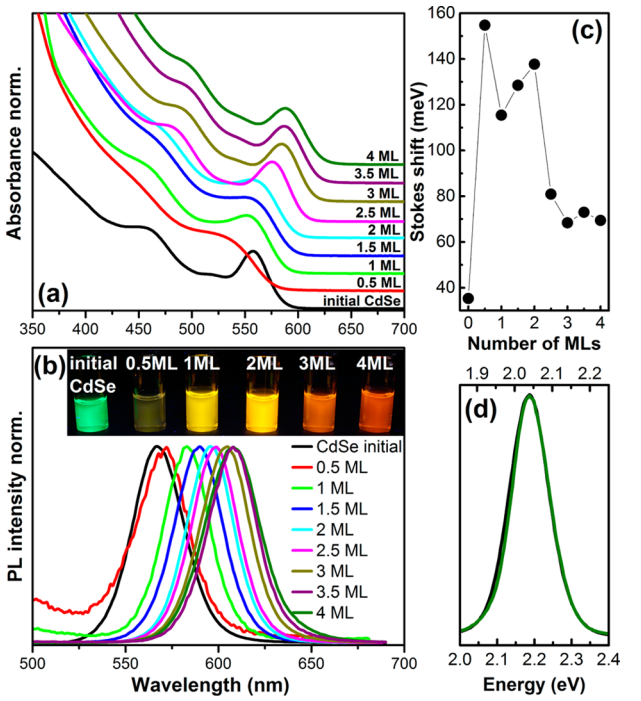

Figure 2. Evolution of the absorption (a) and the PL (b) spectra as well as values of the Stokes shift (c) of CdSe NCs during their alternate shelling with CdS and ZnS forming the CdSe/CdS/ZnS/CdS/ZnS structure. The inset in panel b shows PL color evolution (samples under UV light) during the shelling. (d) PL spectra of the initial CdSe and the final multishell NC structure (plotted on energy scale and superposed to match the peak maxima in the same point) clearly demonstrating that the fwhm was not broadened (0.125 eV for the initial CdSe NCs vs 0.118 eV for the final NC structure).

after the addition of the first half-ML, CdSe/S^{2-}, the first electron transition peak in the absorption spectrum broadens and shifts to shorter wavelengths most probably due to a partial surface etching of the CdSe core. Although addition of the Cd^{2+} layer leads to a remarkable red shift of the peak, its maximum is still blue-shifted relative to that of parent CdSe NCs. Only after adding the second ML (ZnS) one can see a small shift of the absorption maximum to longer wavelengths continued by depositing the third and the fourth shell layers. Despite these unpredictable changes in absorption spectra during deposition

of the first ML, the PL behaves as expected, i.e., the spectral maxima continuously move to longer wavelengths after each step including the first half-ML (Figure 2b). Growth of the last fourth layer does not lead to prominent changes either in absorption of the NCs or in their PL; the positions of both maxima are quite close to those of CdSe/CdS/ZnS/CdS NCs. Apparently, the main changes in absorption spectra, and namely in their shape and positions of the first and the second electron transitions, occur upon addition of the first two S^{2-} layers, when communication between the outer shell layer and the core is most efficient.

Thus, on the example of the formation of CdSe/CdS/ZnS/CdS/ZnS alternated shell structure starting from 3.3 nm CdSe cores, we demonstrate a fine control over the emission wavelength from green-yellow (λ_{max} = 567 nm) to orange-red (λ_{max} = 608 nm) during the growth of either CdS or ZnS shell layers (Figure 2b). The positions of the PL maxima of the other heterostructured NC samples are summarized in Figure SI7. Figure 2d presents a comparison between the PL spectra acquired before and after the c-ALD. The spectral shape, symmetrical profile, and the full-width at half-maximum (fwhm) of the PL spectra can be considered as a measure of the NC size distribution and an overall quality of the particles. One can clearly see that the fwhm value was not altered after the 4 ML shell growth, as compared to that of the initial core sample (the two *x*-axes have been shifted for superposition of the peaks). This observation suggests the preservation of the standard size deviation of the heterostructured NCs under the employed synthesis conditions, a result which is almost unattainable by means of other shell growth techniques.[32] The data presented in Table 1 reveals that the growth process is

Table 1. Evolution of the Crystal Size Dispersion Expressed as FWHM of the PL Spectra (in eV) for Different Shell Compositions

#ML	/CdS4	/CdS/ ZnS/ CdS/ZnS	/ZnS4	/CdS3/ ZnS	/ZnS/ CdS3	/CdS2/ ZnS/ CdS	/CdS2/ ZnS2
0	0.14	0.14	0.10	0.10	0.10	0.10	0.10
0.5	0.14	0.14	0.15			0.15	0.13
1	0.11	0.11		0.13	0.20		0.18
1.5	0.11	0.11	0.16	0.11	0.13	0.10	0.17
2	0.10	0.12	0.12	0.10	0.14	0.10	0.15
2.5	0.10	0.10		0.12	0.14		0.16
3	0.10	0.12	0.14	0.11	0.16	0.10	0.16
3.5	0.10	0.12	0.11	0.14	0.15	0.11	0.17
4	0.12	0.14	0.13	0.15	0.13	0.13	0.16

quite homogeneous, although for some shell compositions we can notice slight broadening of the PL spectra during c-ALD. We note that stability in polar solvents has always been a major issue for NC storage. We noticed a good stability of our purified NCs in MFA (ε_r = 182) only within weeks. The NCs dissolved in other polar solvents, e.g., formamide, (ε_r = 110) precipitated after several hours. The surface functionalization of inorganic-capped NCs with amines enables their colloidal stability to be significantly enhanced as will be demonstrated for Au/CdS core/shell NCs (see below).[30]

In addition to the above-discussed fine-tuning of the absorption and emission spectra, shelling via c-ALD also provides a means to control the Stokes shift of the quantum dots. In the case of the CdSe/CdS/ZnS/CdS/ZnS structure, we see the largest change in the Stokes shift (from 35 to 155 meV) upon depositing the first sulfur layer mostly due to partial NC etching and high concentration of surface defects (Figure 2c). The Stokes shift remains quite large for the first two MLs and then decreases by adding the third and the fourth MLs down to 69 meV, which is still twice larger than the initial value. As in the case of standard shelling procedures, c-ALD results in the overall increase of the PL intensity of the quantum dots demonstrated in Figure SI8. The value of the PL intensity remained almost unaltered during the first ML (ZnS) deposition, thereafter it raised upon adding the next three CdS layers, and its intensity increased 6-fold of the starting value for the parent CdSe NCs going through the maximal enhancement in CdSe/ZnS/CdS2 NC heterostructure (10-fold increase). From the graph we clearly see that PL drops after each S^{2-} layer deposition and goes up upon covering with Cd^{2+}. For example, the PLQY of CdSe/CdS3/ZnS NCs was estimated as 42%, which was much higher compared to that of the initial CdSe NC core (17%; Figure SI9).

Figure 3 shows representative TEM images of the initial 3.8 nm CdSe core NCs and 4.5 nm CdSe/CdS4 core/shell NCs

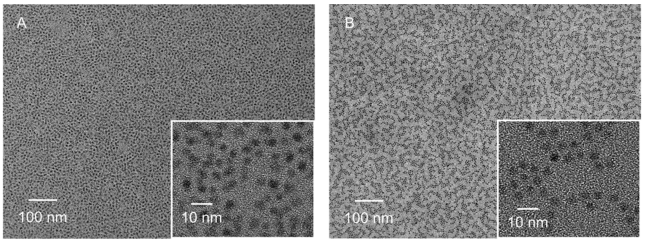

Figure 3. TEM images taken at different magnifications of the initial 3.8 nm core CdSe NCs (A) and the resulting CdSe/ZnS/CdS3 core/shell NCs (B).

revealing their narrow size distribution. This imaging is a good indication of the quality of the shell growth process, which succeeded to preserve NC size distribution, one of the major limitations in obtaining high quality heterostructures by means of solution-based techniques.

The powder XRD patterns of the initial CdSe and CdSe/CdS3/ZnS NCs are presented in Figure 4. The growth of the CdS shell with added 1 ML of ZnS resulted in a narrowing of all reflections and their shift to larger 2θ values due to smaller CdS (ZnS) lattice constant compared to that of CdSe core NCs. The narrowing of the reflections can be explained by a good epitaxial contact between the core and shell materials as well as increasing particle size after shelling.

The combination of two or more semiconductor materials in one multicomponent structure allows us to modulate and control NC functional properties by means of wave function engineering.[7] To evaluate the degree of wave function delocalization, we used the evolution of the $1S_e-1S_h$ exciton transition energy during the shelling process.[7,33,34] From Figure 5a one can distinguish a greater volume extent of the electron wave function for CdSe/CdS4 compared to that of CdSe/CdS/ZnS/CdS/ZnS NCs. The former structure entails the electron delocalization across the entire core−shell particle owing to a low energy barrier between conduction band edges of CdSe and CdS (see Figure 1), while holes are mainly localized within the CdSe core (quasi-Type-II band alignment). The introduction of a thin ZnS layer (1 ML) between two CdS layers partly decouples these two regions leading to a reduced probability of the full delocalization of the electron wave

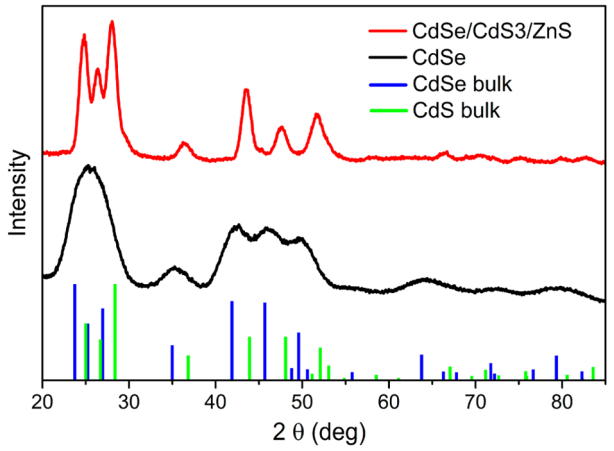

Figure 4. Powder XRD patterns measured for CdSe core and CdSe/CdS3/ZnS heterostructure NCs. The stick patterns show the standard peak positions of the bulk wurtzite CdSe (blue; COD#9011664) and CdS (green; COD#9008862). Note that the thin ZnS shell layer (1 ML) does not change the position of the reflections compared to thicker CdS (3 ML).

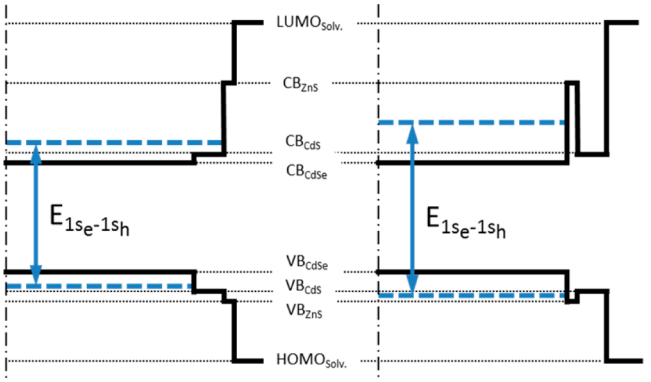

Figure 6. Evolution of the $1S_e-1S_h$ transition for different shell configurations: the presence of ZnS after (left) or before (right) the sequence of three CdS MLs dramatically changes the configuration of the confinement potential. In the latter case, both the hole and especially the electron are more confined, leading to a wider $E_{1Se-1Sh}$ transition, i.e., to a blue shift. This effect would be valid even with an attenuated delocalization of the hole wave function into the CdS shell.

function. Interestingly, the deposition of the same thin 1 ML ZnS (~0.31 nm) shell directly on the CdSe core (in contrast to the above-mentioned ZnS layer that was added on CdS layer) provides a stronger localization of the electrons in the core (Figures 1, 5b, and 6). This weak dependence of charge carrier localization on both core size and the thickness of thin shell layers (1−2 ML) is clearly observed for the other four samples in the CdSe/CdS/ZnS system (Figures SI1−SI6). This is in contrast to the previous results published by the Klimov group for ZnSe/CdSe heterostructures.[35,36] The degree of charge carrier localization was stated to change with the size of each domain, i.e., with core radius and shell thickness, resulting in a modification of the strength and nature of carrier−carrier interactions. The latter led to the transition from standard type I to type II and inverted type I heterostructures in ZnSe/CdSe quantum dots. These discrepancies with the data observed in the current work can be attributed to the larger energy offsets between the core CdSe and the shell ZnS materials (U_o^e = 1.27 eV and U_o^h = 0.60 eV),[8,37] as compared to ZnSe and CdSe (U_o^e = 0.86 eV and U_o^h = 0.14 eV;[35] Figure 1). This results in the strong effect on the localization regime of the carriers in the heterostructures. On other hand, we assume that the larger crystal lattice mismatch between CdSe and ZnS phases can result in the formation of dislocations, additional defects, and interfacial strains, which directly influence the band offset and thus exciton confinement which makes additional contribution to exciton localization.[38] Moreover, the presence of such defects is likely responsible for a remarkable blue shift relative to the initial CdSe NCs (Figures 5b, SI1, and SI4).

The subsequent CdS shell growth extends carrier delocalization as evidenced in the gradual red-shift in the absorption spectra (Figure 5b). As expected, the relaxation of quantum confinement is more pronounced in smaller CdSe NCs as one can compare the electron delocalization from the CdSe core (3.3 nm vs 3.8 nm) into the CdS shell with the same thickness (Figures 5a,b and SI10).

Increasing ZnS content in the shell leads to a larger energy of the transition (lower degree of delocalization experienced by the excited charge carriers), as depicted in Figure 7. The samples are listed in order of increasing the total number of ZnS monolayers within the shell, starting from the pure CdS shell (0 MLs) to the pure ZnS one (4 MLs). Since the incorporation of the ZnS layers causes an increase of electron localization in the conduction band, higher values of the transition energy are associated with a larger content of ZnS in

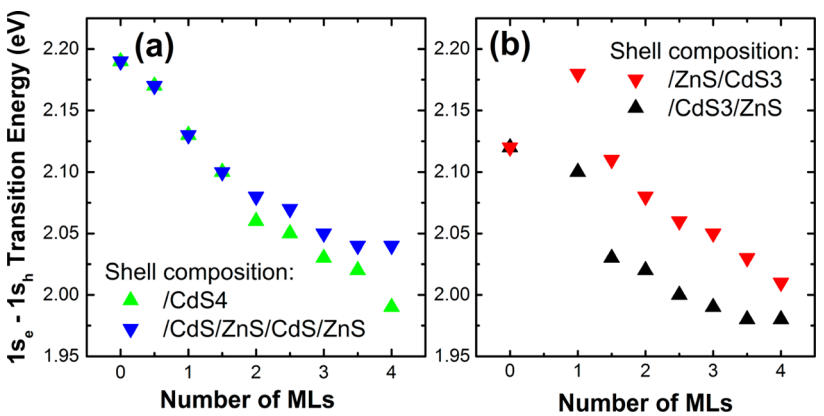

Figure 5. Evolution of the $1S_e-1S_h$ transition energy for different shell configurations: the presence of ZnS within the shell causes a smaller redshift (a) and sequence of the shelling materials influences the transition energy (b).

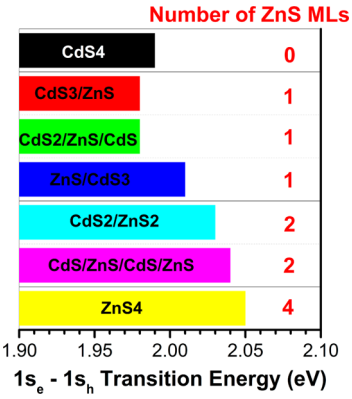

Figure 7. Diagram representing the value of the $1S_e-1S_h$ transition (in eV) for seven different shell combinations: increasing the content of ZnS in the shell leads to a smaller red-shift.

the shell and depend also on the position (distance from the core) of the ZnS layers within the shell structure.

Our results demonstrate that it is possible to grow ZnS shells on CdSe cores via c-ALD in a controlled manner and even to stack multiple instances of different materials without losing coherence and preserving the monodispersity of the starting sample (Table 1). On the other hand, since the shell growth takes place at room temperature, this hampers the achievement of high PL QY in these heterostructures. Nevertheless, the measured PL QY of the core–shell NCs reached as high as 50%. The technique has been evaluated for materials such as cadmium sulfide and zinc sulfide, but its potential extension and versatility to other II–VI compounds is expected, in particular, for the development of other metal sulfide and metal selenide compounds. Indeed, the metal acetate precursors are common chemical reagents in the colloidal synthesis of quantum dots while potassium (ammonium) sulfide/selenide powders are soluble in MFA.

Two-Component Metal–Semiconductor Core/Shell Nanostructures. The colloidal synthesis discussed above enables semiconductor core–shell nanoscale multicomponent structures to be prepared that combine materials with similar functionalities. Additionally, the opportunity to integrate components with intrinsically different characteristics (metal–semiconductor, magnet–semiconductor, etc.) in one nanoscale unit can open a powerful route to functional materials with novel properties. Previously, Zhang et al.[24] demonstrated the fabrication of a wide range of nanoscale heterostructures consisting of a metal core and monocrystalline semiconductor shell with a substantial lattice mismatch between them. However, the method entails a number of tedious synthetic steps strongly controlled by a Lewis acid–base reaction mechanism. On the other hand, we see no obstacles for using c-ALD as an alternative approach to grow a semiconductor shell on a metallic core. Therefore, in this work, we attempted to synthesize Au/CdS core/shell NCs using c-ALD. In a similar manner, using self-limiting half-reactions of S^{2-} and Cd^{2+} on the surface of Au NCs, we created the shell layer with varied CdS thickness of up to 7 ML around the quasi-spherical metal cores. However, in contrast to CdSe-based core/shell NCs, the all-inorganic Au/CdS*n* NCs (*n* is the number of CdS shell MLs) were found to precipitate within a few days regardless of the shell thickness. To improve the colloidal stability of the core/shell NCs, we adapted the technique recently developed by our group.[30] It is based on the ability of amine-functionalized ligands to modify the labile diffusion region of the inorganic-capped NCs. In particular, the surface functionalization of the NCs with OlAm enables to transfer the inorganic-capped NCs from polar (MFA) to nonpolar (toluene) phase.

Figure 8 shows TEM images of starting 4 nm Au cores and the hybrid-capped Au/CdS7 NCs, confirming the formation of

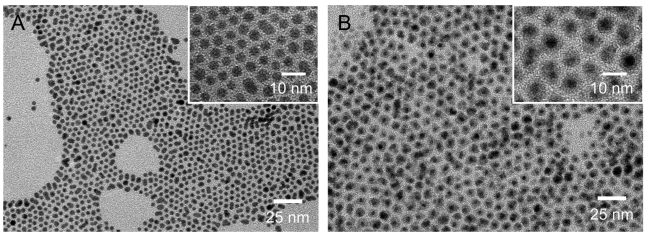

Figure 8. TEM images of the Au cores and the Au/CdS7 core/shell NCs.

a uniform semiconductor layer on the surface of Au via c-ALD. During the CdS shell growth, the average particle diameter increases from 4 to ~8.5 nm, which corresponds to a shell thickness of approximately 2.3 nm, perfectly matching the expected 7 ML thickness of the CdS shell layer. Interestingly, the narrow-size distribution of centrosymmetric Au/CdS7 NCs allowed their self-assembly into ordered structures.

CdS shell growth on gold cores has been monitored by absorption spectroscopy during c-ALD. The localized surface plasmon resonance (LSPR) peak gradually broadened and red-shifted with increasing CdS shell thickness (Figure 9a). Particularly, the LSPR maximum shifted from 512 nm in bare Au NCs to 618 nm in Au/CdS7 core/shell NCs. Such behavior can be explained by the increase of the effective dielectric constant around plasmonic NCs with increasing shell thickness.[22] The enhanced plasmon–exciton interaction can lead to the spectral broadening of the LSPR. The increased absorption cross-section at energies higher than the CdS band gap (~510 nm) is consistent with the formation of a CdS shell, as one can clearly see already for Au/CdS3 NCs. The presence of the LSPR peak after the deposition of the multiple shell layers is a clear indication that gold cores have preserved their integrity during the process, irrespective to the amount of the shell formed.[39] No light is emitted by gold–cadmium sulfide core–shell structures, as the Au Fermi level lays below the CdS conduction band that promotes the charge transfer toward the metal core causing the quenching of the emission of this structure.[40]

The XRD patterns revealed the presence of characteristic reflexes of fcc Au and hexagonal CdS phases (Figure 9b). The larger fraction of CdS in Au/CdS7 than in Au/CdS3 NCs is reflected in the enhanced intensity of (100) and (101) as well as (112) peaks at 2θ = 24.9°, 2θ = 28.2°, and 2θ = 51.9°, respectively. This opportunity of the formation of the highly crystalline shell layers around the core NCs with large lattice mismatch at room temperature opens up new perspectives for the c-ALD approach to synthesize diverse heterostructures with tunable compositional complexity and properties.

CONCLUSIONS

Complex multifunctional nanoscale materials with similar and different properties were successfully synthesized using the c-ALD technique. All core–shell multicomponent nanoparticles

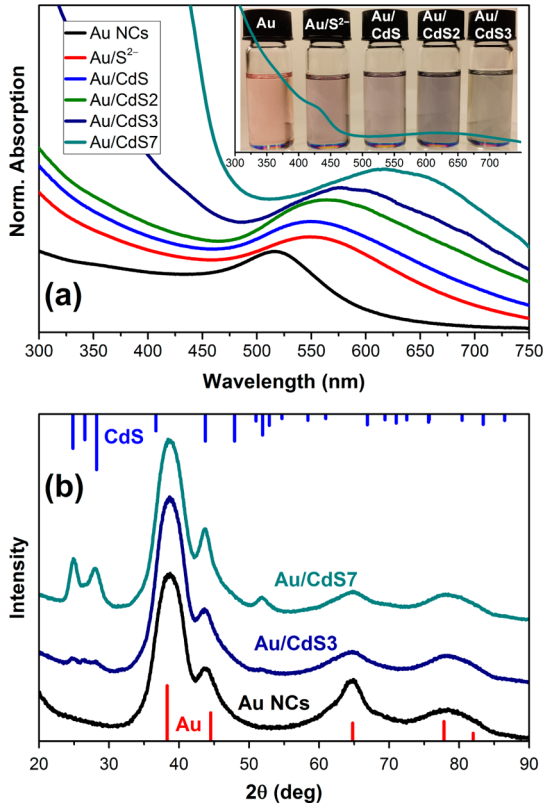

Figure 9. (a) Absorption spectra of the initial Au core (with diameter of ~4 nm) and core/shell Au/CdS NCs with varied shell thickness functionalized with oleylamine and dissolved in toluene. The spectra are normalized by the LSPR maxima and vertically shifted for clarity. The inset shows a full spectrum of the Au/CdS7 NCs demonstrating a clear absorption of the CdS shell (a shoulder between 400 and 450 nm) and a photo of the NC dispersions. (b) Powder XRD patterns of the Au core, Au/CdS3, and Au/CdS7 core/shell NCs exhibiting all reflections expected from the fcc Au and wurtzite CdS crystal structures. The stick patterns show the standard peak positions of the bulk Au (bottom red sticks, COD#9012953) and CdS (top blue sticks, COD#9008862).

preserve the narrow size distributions, phase crystallinity, and shape homogeneity of the initial NCs. Particularly, uniform layers of CdS and ZnS semiconductor shells were epitaxially grown on CdSe semiconductor cores with different shell combinations leading to an unprecedented control of optical properties of these heterostructures. The shell growth of the CdS semiconductor phase on a metal Au core was additionally demonstrated, implying the general applicability of the method to synthesize complex structures with substantial lattice mismatch. The results presented in this work demonstrate great potential for creating functional materials with new properties for practical applications.

■ ASSOCIATED CONTENT

Supporting Information

The Supporting Information is available free of charge on the ACS Publications website at DOI: 10.1021/acs.chemmater.7b01873.

Additional absorption and PL spectra of the NC heterostructures, graphs summarizing PL maxima shifts, PL intensity evolution, and electron transition energy changes. (PDF)

■ AUTHOR INFORMATION

Corresponding Author

*E-mail: vladimir.lesnyak@chemie.tu-dresden.de.

ORCID

Emanuele A. Slejko: 0000-0003-4946-2612
Bin Cai: 0000-0002-3263-0395
Nikolai Gaponik: 0000-0002-8827-2881
Vladimir Lesnyak: 0000-0002-2480-8755
Alexander Eychmüller: 0000-0001-9926-6279

Author Contributions

§E.A.S. and V.S. contributed equally to the work.

Notes

The authors declare no competing financial interest.

■ ACKNOWLEDGMENTS

We are grateful to S. Goldberg (TU Dresden) for TEM imaging. E.A.S. acknowledges the support by the Erasmus + Traineeship Programme for Higher Education. V.S. acknowledges the support from the Project 100315856 BacMot, Sächsische Aufbaubank. This work was supported by the German Research Foundation (DFG) within the Cluster of Excellence "Center for Advancing Electronics Dresden" (cfAED) and within the M-ERA.NET Project ICENAP (GA1289/3-1).

■ REFERENCES

(1) Talapin, D. V.; Lee, J.-S.; Kovalenko, M. V.; Shevchenko, E. V. Prospects of Colloidal Nanocrystals for Electronic and Optoelectronic Applications. *Chem. Rev.* **2010**, *110*, 389−458.

(2) Kovalenko, M. V.; Manna, L.; Cabot, A.; Hens, Z.; Talapin, D. V.; Kagan, C. R.; Klimov, V. I.; Rogach, A. L.; Reiss, P.; Milliron, D. J.; et al. Prospects of Nanoscience with Nanocrystals. *ACS Nano* **2015**, *9*, 1012−1057.

(3) Saldanha, P. L.; Lesnyak, V.; Manna, L. Large Scale Syntheses of Colloidal Nanomaterials. *Nano Today* **2017**, *12*, 46−63.

(4) Donegá, C. de M. Synthesis and Properties of Colloidal Heteronanocrystals. *Chem. Soc. Rev.* **2011**, *40*, 1512−1546.

(5) Cozzoli, P. D.; Pellegrino, T.; Manna, L. Synthesis, Properties and Perspectives of Hybrid Nanocrystal Structures. *Chem. Soc. Rev.* **2006**, *35*, 1195−1208.

(6) Dorfs, D.; Eychmüller, A. A Series of Double Well Semiconductor Quantum Dots. *Nano Lett.* **2001**, *1*, 663−665.

(7) Mews, A.; Eychmüller, A. Quantum Wells within Quantum Dots, a CdS/HgS Nanoheterostructure with Global and Local Confinement. *Ber. Bunsenges. Phys. Chem.* **1998**, *102*, 1343−1357.

(8) Reiss, P.; Protière, M.; Li, L. Core/Shell Semiconductor Nanocrystals. *Small* **2009**, *5*, 154−168.

(9) Ghosh Chaudhuri, R.; Paria, S. Core/Shell Nanoparticles: Classes, Properties, Synthesis Mechanisms, Characterization, and Applications. *Chem. Rev.* **2012**, *112*, 2373−2433.

(10) Guo, Y.; Marchuk, K.; Sampat, S.; Abraham, R.; Fang, N.; Malko, A. V.; Vela, J. Unique Challenges Accompany Thick-Shell CdSe/nCdS (n > 10) Nanocrystal Synthesis. *J. Phys. Chem. C* **2012**, *116*, 2791−2800.

(11) Talapin, D. V.; Mekis, I.; Götzinger, S.; Kornowski, A.; Benson, O.; Weller, H. CdSe/CdS/ZnS and CdSe/ZnSe/ZnS Core−Shell−Shell Nanocrystals. *J. Phys. Chem. B* **2004**, *108*, 18826−18831.

(12) Chen, O.; Zhao, J.; Chauhan, V. P.; Cui, J.; Wong, C.; Harris, D. K.; Wei, H.; Han, H.-S.; Fukumura, D.; Jain, R. K.; et al. Compact High-Quality CdSe−CdS Core−Shell Nanocrystals with Narrow Emission Linewidths and Suppressed Blinking. *Nat. Mater.* **2013**, *12*, 445−451.

(13) Boldt, K.; Kirkwood, N.; Beane, G. A.; Mulvaney, P. Synthesis of Highly Luminescent and Photo-Stable, Graded Shell CdSe/$Cd_xZn_{1-x}S$ Nanoparticles by In Situ Alloying. *Chem. Mater.* **2013**, *25*, 4731−4738.

(14) Chen, D.; Zhao, F.; Qi, H.; Rutherford, M.; Peng, X. Bright and Stable Purple/Blue Emitting CdS/ZnS Core/Shell Nanocrystals Grown by Thermal Cycling Using a Single-Source Precursor. *Chem. Mater.* **2010**, *22*, 1437−1444.
(15) Nan, W.; Niu, Y.; Qin, H.; Cui, F.; Yang, Y.; Lai, R.; Lin, W.; Peng, X. Crystal Structure Control of Zinc-Blende CdSe/CdS Core/Shell Nanocrystals: Synthesis and Structure-Dependent Optical Properties. *J. Am. Chem. Soc.* **2012**, *134*, 19685−19693.
(16) Li, J. J.; Wang, Y. A.; Guo, W.; Keay, J. C.; Mishima, T. D.; Johnson, M. B.; Peng, X. Large-Scale Synthesis of Nearly Monodisperse CdSe/CdS Core/Shell Nanocrystals Using Air-Stable Reagents via Successive Ion Layer Adsorption and Reaction. *J. Am. Chem. Soc.* **2003**, *125*, 12567−12575.
(17) Ithurria, S.; Talapin, D. V. Colloidal Atomic Layer Deposition (c-ALD) Using Self-Limiting Reactions at Nanocrystal Surface Coupled to Phase Transfer between Polar and Nonpolar Media. *J. Am. Chem. Soc.* **2012**, *134*, 18585−18590.
(18) Razgoniaeva, N.; Carrillo, L.; Burchfield, D.; Moroz, P.; Adhikari, P.; Yadav, P.; Khon, D.; Zamkov, M. Colloidal Synthesis of Monodisperse Semiconductor Nanocrystals through Saturated Ionic Layer Adsorption. *Chem. Mater.* **2016**, *28*, 2823−2833.
(19) Sagar, L. K.; Walravens, W.; Zhao, Q.; Vantomme, A.; Geiregat, P.; Hens, Z. PbS/CdS Core/Shell Quantum Dots by Additive, Layer-by-Layer Shell Growth. *Chem. Mater.* **2016**, *28*, 6953−6959.
(20) She, C.; Fedin, I.; Dolzhnikov, D. S.; Demortière, A.; Schaller, R. D.; Pelton, M.; Talapin, D. V. Low-Threshold Stimulated Emission Using Colloidal Quantum Wells. *Nano Lett.* **2014**, *14*, 2772−2777.
(21) Oh, S. J.; Berry, N. E.; Choi, J.-H.; Gaulding, E. A.; Lin, H.; Paik, T.; Diroll, B. T.; Muramoto, S.; Murray, C. B.; Kagan, C. R. Designing High-Performance PbS and PbSe Nanocrystal Electronic Devices through Stepwise, Post-Synthesis, Colloidal Atomic Layer Deposition. *Nano Lett.* **2014**, *14*, 1559−1566.
(22) Lee, J.; Shevchenko, E. V.; Talapin, D. V. Au−PbS Core−Shell Nanocrystals: Plasmonic Absorption Enhancement and Electrical Doping via Intra-Particle Charge Transfer. *J. Am. Chem. Soc.* **2008**, *130*, 9673−9675.
(23) Park, J.; Joo, J.; Kwon, S. G.; Jang, Y.; Hyeon, T. Synthesis of Monodisperse Spherical Nanocrystals. *Angew. Chem., Int. Ed.* **2007**, *46*, 4630−4660.
(24) Zhang, J.; Tang, Y.; Lee, K.; Ouyang, M. Nonepitaxial Growth of Hybrid Core-Shell Nanostructures with Large Lattice Mismatches. *Science* **2010**, *327*, 1634−1638.
(25) Murray, C. B.; Norris, D.; Bawendi, M. G. Synthesis and Characterization of Nearly Monodisperse CdE (E= S, Se, Te) Semiconductor Nanocrystallites. *J. Am. Chem. Soc.* **1993**, *115*, 8706−8715.
(26) Bullen, C.; Mulvaney, P. Nucleation and Growth Kinetics of CdSe Nanocrystals in Octadecene. *Nano Lett.* **2004**, *4*, 2303−2307.
(27) Carbone, L.; Nobile, C.; De Giorgi, M.; Sala, F.; Morello, G.; Pompa, P.; Hytch, M.; Snoeck, E.; Fiore, A.; Franchini, I. R.; et al. Synthesis and Micrometer-Scale Assembly of Colloidal CdSe/CdS Nanorods Prepared by a Seeded Growth Approach. *Nano Lett.* **2007**, *7*, 2942−2950.
(28) Peng, S.; Lee, Y.; Wang, C.; Yin, H.; Dai, S.; Sun, S. A Facile Synthesis of Monodisperse Au Nanoparticles and Their Catalysis of CO Oxidation. *Nano Res.* **2008**, *1*, 229−234.
(29) Jasieniak, J.; Smith, L.; van Embden, J.; Mulvaney, P.; Califano, M. Re-Examination of the Size-Dependent Absorption Properties of CdSe Quantum Dots. *J. Phys. Chem. C* **2009**, *113*, 19468−19474.
(30) Sayevich, V.; Guhrenz, C.; Dzhagan, V. M.; Sin, M.; Werheid, M.; Cai, B.; Borchardt, L.; Widmer, J.; Zahn, D. R. T.; Brunner, E.; et al. Hybrid N -Butylamine-Based Ligands for Switching the Colloidal Solubility and Regimentation of Inorganic-Capped Nanocrystals. *ACS Nano* **2017**, *11*, 1559−1571.
(31) Grabolle, M.; Spieles, M.; Lesnyak, V.; Gaponik, N.; Eychmüller, A.; Resch-Genger, U. Determination of the Fluorescence Quantum Yield of Quantum Dots: Suitable Procedures and Achievable Uncertainties. *Anal. Chem.* **2009**, *81*, 6285−6294.
(32) Boldt, K. Graded Shells in Semiconductor Nanocrystals. *Z. Phys. Chem.* **2017**, *231*, 77−92.
(33) Eychmüller, A.; Mews, A.; Weller, H. A Quantum Dot Quantum Well: CdS/HgS/CdS. *Chem. Phys. Lett.* **1993**, *208*, 59−62.
(34) Pietryga, J. M.; Park, Y.-S.; Lim, J.; Fidler, A. F.; Bae, W. K.; Brovelli, S.; Klimov, V. I. Spectroscopic and Device Aspects of Nanocrystal Quantum Dots. *Chem. Rev.* **2016**, *116*, 10513−10622.
(35) Ivanov, S. A.; Nanda, J.; Piryatinski, A.; Achermann, M.; Balet, L. P.; Bezel, I. V.; Anikeeva, P. O.; Tretiak, S.; Klimov, V. I. Light Amplification Using Inverted Core/Shell Nanocrystals: Towards Lasing in the Single-Exciton Regime. *J. Phys. Chem. B* **2004**, *108*, 10625−10630.
(36) Piryatinski, A.; Ivanov, S. A.; Tretiak, S.; Klimov, V. I. Effect of Quantum and Dielectric Confinement on the Exciton-Exciton Interaction Energy in Type II Core/Shell Semiconductor Nanocrystals. *Nano Lett.* **2007**, *7*, 108−115.
(37) Wei, S.-H.; Zunger, A. Calculated Natural Band Offsets of All II−VI and III−V Semiconductors: Chemical Trends and the Role of Cation d Orbitals. *Appl. Phys. Lett.* **1998**, *72*, 2011−2013.
(38) Smith, A. M.; Mohs, A. M.; Nie, S. Tuning the Optical and Electronic Properties of Colloidal Nanocrystals by Lattice Strain. *Nat. Nanotechnol.* **2009**, *4*, 56−63.
(39) Lambright, S.; Butaeva, E.; Razgoniaeva, N.; Hopkins, T.; Smith, B.; Perera, D.; Corbin, J.; Khon, E.; Thomas, R.; Moroz, P.; et al. Enhanced Lifetime of Excitons in Nonepitaxial Au/CdS Core/Shell Nanocrystals. *ACS Nano* **2014**, *8*, 352−361.
(40) Kahane, S. V.; Sudarsan, V.; Mahamuni, S. Anomalous Photoluminescence Enhancement due to Hot Electron Transfer in Core−Shell Au−CdS Nanocrystals. *J. Lumin.* **2017**, *181*, 91−95.